



Magnetic Fields in a Sample of Planet-hosting M Dwarf Stars from Kepler, K2, and TESS Observed by APOGEE

Fábio Wanderley¹, Katia Cunha^{1,2}, Verne V. Smith³, Oleg Kochukhov⁴, Diogo Souto⁵, C. Allende Prieto^{6,7},
Suvrath Mahadevan^{8,9}, Steven R. Majewski¹⁰, Philip S. Muirhead¹¹, Marc Pinsonneault¹², and Ryan Terrien¹³

¹ Observatório Nacional/MCTIC, R. Gen. José Cristino, 77, 20921-400, Rio de Janeiro, Brazil; fabiowanderley@on.br

² Steward Observatory, University of Arizona, 933 N. Cherry Avenue, Tucson, AZ 85721-0065, USA

³ NSF's NOIRLab, 950 N. Cherry Avenue, Tucson, AZ 85719, USA

⁴ Department of Physics and Astronomy, Uppsala University, Box 516, S-75120 Uppsala, Sweden

⁵ Departamento de Física, Universidade Federal de Sergipe, Avenida Marcelo Deda Chagas, S/N Cep 49.107-230, São Cristóvão, SE, Brazil

⁶ Instituto de Astrofísica de Canarias, E-38205 La Laguna, Tenerife, Spain

⁷ Departamento de Astrofísica, Universidad de La Laguna, E-38206 La Laguna, Tenerife, Spain

⁸ Department of Astronomy & Astrophysics, Pennsylvania State, 525 Davey Lab, University Park, PA 16802, USA

⁹ Center for Exoplanets & Habitable Worlds, Pennsylvania State, 525 Davey Lab, University Park, PA 16802, USA

¹⁰ Department of Astronomy, University of Virginia, Charlottesville, VA 22904-4325, USA

¹¹ Institute for Astrophysical Research and Department of Astronomy, Boston University, 725 Commonwealth Avenue, Boston, MA 02215, USA

¹² Department of Astronomy, The Ohio State University, Columbus, OH 43210, USA

¹³ Department of Physics & Astronomy, Carleton College, Northfield, MN 55057, USA

Received 2024 June 24; revised 2024 September 6; accepted 2024 September 7; published 2024 October 29

Abstract

Stellar magnetic fields have a major impact on space weather around exoplanets orbiting low-mass stars. From an analysis of Zeeman-broadened Fe I lines measured in near-infrared SDSS/APOGEE spectra, mean magnetic fields are determined for a sample of 29 M dwarf stars that host closely orbiting small exoplanets. The calculations employed the radiative transfer code Synmast and MARCS stellar model atmospheres. The sample M dwarfs are found to have measurable mean magnetic fields ranging between ~ 0.2 and ~ 1.5 kG, falling in the unsaturated regime on the $\langle B \rangle$ versus P_{rot} plane. The sample systems contain 43 exoplanets, which include 23 from Kepler, nine from K2, and nine from Transiting Exoplanet Survey Satellite. We evaluated their equilibrium temperatures, insolation, and stellar habitable zones and found that only Kepler-186f and TOI-700d are inside the habitable zones of their stars. Using the derived values of $\langle B \rangle$ for the stars Kepler-186 and TOI-700 we evaluated the minimum planetary magnetic field that would be necessary to shield the exoplanets Kepler-186f and TOI-700d from their host star's winds, considering reference magnetospheres with sizes equal to those of the present-day and young Earth, respectively. Assuming a ratio of 5% between large- to small-scale B -fields, and a young-Earth magnetosphere, Kepler-186f and TOI-700d would need minimum planetary magnetic fields of, respectively, 0.05 and 0.24 G. These values are considerably smaller than Earth's magnetic field of $0.25 \text{ G} \lesssim B \lesssim 0.65 \text{ G}$, which suggests that these two exoplanets might have magnetic fields sufficiently strong to protect their atmospheres and surfaces from stellar magnetic fields.

Unified Astronomy Thesaurus concepts: Near infrared astronomy (1093); M dwarf stars (982); Stellar activity (1580); Stellar magnetic fields (1610)

1. Introduction

M dwarfs are the most abundant stellar type in the Galaxy (E. E. Salpeter 1955; I. N. Reid & J. E. Gizis 1997) and also host the largest reservoir of small planets (A. W. Howard et al. 2012; G. D. Mulders et al. 2015). Given their small sizes, M dwarfs are prime targets for the detection of Terrestrial-type planets, via both transit and radial velocity surveys (A. L. Shields et al. 2016). In addition, the low surface temperatures and luminosities of M dwarfs ($L_{\text{bol}} \lesssim 0.07 L_{\odot}$) result in habitable zones (HZ), defined here as the region where liquid water can be sustained, that are much closer to the host star (e.g., R. K. Kopparapu et al. 2013) when compared to the HZ of FGK dwarfs. However, the fact that a planet around an M dwarf is in the habitable zone does not mean that the planet is habitable (F. Gallet et al. 2017). An important facet of M-dwarf

stars is that they have longer spin-down timescales than hotter main-sequence stars and they maintain intense magnetic fields for longer periods (E. R. Newton et al. 2016) that can, in turn, affect the evolution of planetary atmospheres and surfaces.

Stellar magnetic fields are a key ingredient in driving and shaping stellar winds, flare variability, and high-energy radiation (UV and X-ray) from cool dwarf stars with significant outer convective envelopes. The propagation of high-energy radiation and high-temperature plasma on the circumstellar environment away from the star, also referred to as space weather, impacts the environment of any orbiting planet (E. L. Shkolnik & T. S. Barman 2014). Several works have modeled stellar winds via magnetohydrodynamic simulations to study space weather on M-dwarf planets (e.g., A. A. Vidotto et al. 2014; J. D. Alvarado-Gómez et al. 2019; L. M. Harbach et al. 2021). In particular, the relative strengths of the magnetic fields of the star and planet determine, for example, how important planetary atmospheric erosion will be, while changing magnetic field strengths will impact the planet's mass loss rates (S. Gupta et al. 2023).



Original content from this work may be used under the terms of the [Creative Commons Attribution 4.0 licence](https://creativecommons.org/licenses/by/4.0/). Any further distribution of this work must maintain attribution to the author(s) and the title of the work, journal citation and DOI.

Ultimately, the magnetic field of the host star will have an impact on the possible habitability of planets. For example, previous works have modeled space weather around the M dwarf Proxima Centauri, which has a large-scale magnetic field (derived from Zeeman doppler imaging, based on circular polarimetry) (B_{ZDI}) = 200 G (B. Klein et al. 2021). C. Garraffo et al. (2022), using the magnetic field determinations from B. Klein et al. (2021), found that the exoplanet Proxima Centauri b (semimajor axis of $a = 0.049$ au), which falls in the HZ, could support a planetary magnetosphere for planetary magnetic fields of $B_p = 0.1$ G, while J. D. Alvarado-Gómez et al. (2020) found an “Earth-like” stellar wind environment around the exoplanet Proxima Centauri c ($a = 1.44$ au), given the weak interplanetary magnetic field at the distance of this planet. However, at the distance of Proxima Centauri d ($a = 0.029$ au), the closest orbiting planet in the Proxima Cen system, the conditions were likely extremely adverse. Finally, habitability will also depend on planetary magnetic fields, as these can shield the atmosphere and the surface of the planet (A. A. Vidotto et al. 2013).

In this study, we determine mean magnetic fields for a sample of 29 planet-hosting, partially convective, M (and some late-K) dwarfs by modeling Zeeman intensified Fe I lines in SDSS APOGEE spectra (S. R. Majewski et al. 2017). This stellar sample contains, in total, 23 exoplanets that were detected by the Kepler mission (W. J. Borucki et al. 2010; D. G. Koch et al. 2010; N. M. Batalha et al. 2013), nine exoplanets detected by K2 (S. B. Howell et al. 2014), nine exoplanets detected by Transiting Exoplanet Survey Satellite (TESS; G. R. Ricker et al. 2015), one exoplanet detected with the HARPS spectrograph (M. Mayor et al. 2003) via the radial velocity method, and one exoplanet that was detected using data from multiple observatories via transit timing variation (TTV), for a total sample of 43 exoplanets.

This paper is organized as follows: in Section 2, we present the sample of planet-hosting stars analyzed in this study, in Section 3, we discuss the methodology adopted for the mean magnetic field determination, and in Section 4, we present and discuss the results, which include an analysis of the derived magnetic fields as a function of rotational periods, and a discussion about the minimum planetary magnetic field necessary to deflect stellar coronal winds. Finally, Section 5 summarizes the conclusions.

2. Observations and the Sample

Our spectroscopic analysis is based on near-infrared ($\lambda 1.51 \mu\text{m}$ to $\lambda 1.69 \mu\text{m}$), high-resolution (average resolution of $R \sim 22,500$) spectra of M-dwarf stars observed by the SDSS III and IV APOGEE survey (M. R. Blanton et al. 2017; S. R. Majewski et al. 2017). The APOGEE spectra were obtained using the 300-fiber multiobject spectrographs located at two 2.5 m telescopes, with one at the Apache Point Observatory in the Northern Hemisphere, and the other at Las Campanas Observatory in the Southern Hemisphere (I. S. Bowen & A. H. J. Vaughan 1973; J. E. Gunn et al. 2006; J. C. Wilson et al. 2019).

The stellar sample in this study was defined by cross-matching M-dwarf stars from the APOGEE Data Release 17 (DR17; Abdurro’uf et al. 2022) with $T_{\text{eff}} < 4000$ K, with the table of confirmed planets and host stars from the NASA Exoplanet Archive. We consider only stars unlikely to be members of binary or multiple systems by restricting the

sample to those having values of Gaia DR3 (Gaia Collaboration 2016, 2023) RUWE < 1.4 (V. Belokurov et al. 2020). We also checked the literature to remove stars known to be members of binary or multiple systems, and, in addition, we examined the radial velocity scatter for stars that were observed more than once with APOGEE, removing stars with a radial velocity scatter greater than 1 km s^{-1} . The final stellar sample whose magnetic fields were determined in this study is composed of the 29 M-dwarf stars presented in Table 1. Within this final sample of 29 stars and 43 exoplanets, 22 of the stellar hosts have a single detected planet, while seven of them host more than one detected planet: Kepler-186 has five exoplanets, TOI-700 has four exoplanets, Kepler-138 has four exoplanets, and TOI-2095, Kepler-732, Kepler-1350, and K2-83 have two detected exoplanets each.

3. Mean Magnetic Fields Determination

The mean magnetic fields for the sample of M dwarfs were derived by employing the same methodology described in F. Wanderley et al. (2024). We measured the Zeeman effect in four selected Fe I lines at $\lambda 15207.526 \text{ \AA}$, $\lambda 15294.56 \text{ \AA}$, $\lambda 15621.654 \text{ \AA}$, and $\lambda 15631.948 \text{ \AA}$, which have effective Landé g factors of, respectively, 1.532, 1.590, 1.494, and 1.655, according to the VALD database (N. E. Piskunov et al. 1995; F. Kupka et al. 1999), making them sensitive lines to magnetic fields. The stellar parameters (effective temperatures, surface gravities, and stellar radii) for the sample were obtained using the procedure described in our previous studies (D. Souto et al. 2020; F. Wanderley et al. 2023). We derived projected stellar rotational velocities ($v \sin i$) using OH lines, keeping in mind that these are insensitive to magnetic fields (see F. Wanderley et al. 2024).

Given the adopted stellar parameters, for each star, we generated a spectral synthesis grid for the selected Fe I lines, with $\langle B \rangle$ values ranging from 2 to 6 kG with a 2 kG step, and metallicities $[M/H]$ varying from -0.75 to $+0.5$ with a 0.25 step. This synthetic grid was constructed using the Synmast spectral synthesis code (O. Kochukhov et al. 2010), the APOGEE DR17 line list (V. V. Smith et al. 2021), and MARCS model atmospheres (B. Gustafsson et al. 2008). Each synthesis was convolved with the derived stellar $v \sin i$ using a rotational profile, and with a Gaussian profile corresponding to the LSF of each fiber of the corresponding APOGEE spectrum (see, D. L. Nidever et al. 2015; J. C. Wilson et al. 2019).

We employed a Monte Carlo and Markov Chain (MCMC) methodology for the derivation of mean magnetic fields for the stars, using the python code emcee (D. Foreman-Mackey et al. 2013) to search for the ensemble of filling factors (varying $\langle B \rangle$ between 2 and 6 kG in a 2 kG step) and metallicity that best fits the four Fe I lines. Each group of parameters has an associated $\langle B \rangle$ value given by:

$$\langle B \rangle = \sum_n f_n \times 1000n, \quad n = [2, 4, 6]. \quad (1)$$

The mean magnetic fields were given by the median of the posterior distribution of $\langle B \rangle$, with the lower and upper uncertainties given, respectively, by the 16th and 84th percentiles (Table 1). Figure 1 shows the results for the target M dwarf 2M07590587+1523294, where the left panels present comparisons between the model and observations, and best-fit results for the four studied Fe I lines are shown as blue lines. Black dots represent the observed APOGEE spectrum, and red

Table 1
Stellar and Planetary Results

APOGEE ID ...	Exoplanet ...	$\langle B \rangle$ (G)	ϕ_B (10^{25} Mx)	P_{rot} (days)	OHZ (au)	IHZ ^a (au)	a (au)	T_{eq} (K)	S_p (S_{\oplus})	$B_{p,\text{min}}^b$ (G)	$B_{p,\text{min}}^c$ (G)
2M00391724+0716375	K2-149 b	402^{+122}_{-115}	0.813	...	0.503	0.264	0.083	447	9.45	0.33/1.67/3.34	4.28/21.41/42.83
2M03593637+1533320	K2-83 b	695^{+230}_{-217}	1.119	...	0.473	0.249	0.031	711	60.51	3.28/16.42/32.85	42.09/210.43/420.86
2M03593637+1533320	K2-83 c	695^{+230}_{-217}	1.119	...	0.473	0.249	0.074	462	10.77	0.58/2.92/5.84	7.49/37.44/74.89
2M04342248+4302148	TOI-1685 b	418^{+194}_{-165}	0.513	18.66	0.344	0.178	0.012	981	219.23	10.88/54.41/108.81	139.42/697.12/1394.24
2M04545692-6231205	TOI-206 b	1458^{+402}_{-410}	1.017	...	0.243	0.125	0.011	834	114.62	22.97/114.85/229.71	294.32/1471.6/2943.2
2M06282325-6534456	TOI-700 d	439^{+248}_{-194}	0.443	54	0.307	0.158	0.163	246	0.87	0.05/0.24/0.47	0.6/3.02/6.04
2M06282325-6534456	TOI-700 c	439^{+248}_{-194}	0.443	54	0.307	0.158	0.093	326	2.69	0.15/0.73/1.46	1.87/9.33/18.65
2M06282325-6534456	TOI-700 b	439^{+248}_{-194}	0.443	54	0.307	0.158	0.068	382	5.06	0.27/1.37/2.74	3.51/17.56/35.12
2M06282325-6534456	TOI-700 e	439^{+248}_{-194}	0.443	54	0.307	0.158	0.134	272	1.29	0.07/0.35/0.7	0.9/4.48/8.96
2M07590587+1523294	GJ 3470 b	740^{+153}_{-155}	1.115	21.54	0.397	0.206	0.036	603	31.23	2.51/12.53/25.06	32.11/160.54/321.07
2M08255432+2021344	K2-122 b	271^{+86}_{-83}	0.576	29.37	0.544	0.287	0.029	791	92.53	1.95/9.76/19.53	25.02/125.09/250.18
2M08372705+1858360	K2-95 b	1262^{+401}_{-383}	1.358	23.9	0.302	0.155	0.065	386	5.23	0.9/4.51/9.02	11.56/57.81/115.63
2M08383283+1946256	K2-104 b	641^{+273}_{-233}	0.875	9.3	0.391	0.204	0.024	736	69.53	4.45/22.25/44.51	57.03/285.14/570.28
2M09052674+2140075	K2-344 b	343^{+112}_{-106}	0.566	...	0.475	0.25/.../...	.../.../...
2M09533093+3534171	Wolf 327 b	331^{+201}_{-151}	0.316	44.4	0.301	0.155	0.01	986	224.08	8.94/44.71/89.41	114.56/572.81/1145.62
2M10302934+0651492	K2-324 b	674^{+195}_{-187}	0.973	...	0.408	0.212	0.033	635	38.46	2.52/12.58/25.16	32.23/161.17/322.34
2M10374104+0617094	K2-323 b	188^{+107}_{-84}	0.299	...	0.429	0.223	0.128	332	2.87	0.05/0.26/0.52	0.67/3.34/6.68
2M18543080+4823277	Kepler-1651 b	518^{+192}_{-173}	0.748	18.18	0.389	0.202	0.062	452	9.9	0.55/2.77/5.53	7.09/35.43/70.86
2M18545568+4557315	Kepler-732 c	192^{+100}_{-81}	0.268	36.14	0.4	0.208	0.014	966	206.49	3.88/19.39/38.78	49.68/248.42/496.83
2M18545568+4557315	Kepler-732 b	192^{+100}_{-81}	0.268	36.14	0.4	0.208	0.068	439	8.83	0.17/0.83/1.66	2.12/10.62/21.25
2M18545777+4730586	Kepler-617 b	718^{+232}_{-218}	1.193	38.27	0.441	0.23	0.022	815	104.19	7.11/35.57/71.14	91.15/455.73/911.47
2M18575437+4615092	Kepler-1074 b	532^{+153}_{-142}	1.019	30.65	0.522	0.275	0.053	572	25.4	1.03/5.14/10.28	13.17/65.83/131.67
2M18594123+4558206	Kepler-504 b	759^{+284}_{-255}	0.66	44.16	0.303	0.157	0.064	392	5.6	0.45/2.27/4.55	5.83/29.14/58.28
2M19000314+4013147	Kepler-974 b	806^{+153}_{-153}	1.278	35.25	0.423	0.22	0.04	592	29.05	2.32/11.61/23.21	29.74/148.69/297.39
2M19023192+7525070	TOI-2095c	576^{+185}_{-176}	0.693	40	0.369	0.192	0.138	296	1.82	0.1/0.52/1.04	1.33/6.65/13.31
2M19023192+7525070	TOI-2095 b	576^{+185}_{-176}	0.693	40	0.369	0.192	0.101	346	3.38	0.19/0.96/1.93	2.47/12.33/24.67
2M19034293+3831155	Kepler-1308 b	324^{+152}_{-130}	0.423	33.95	0.365	0.189	0.023	722	64.49	2.33/11.63/23.26	29.8/149.01/298.03
2M19062262+3753285	Kepler-1124 b	535^{+186}_{-170}	0.729	28.73	0.414	0.217	0.031	664	46	2.16/10.82/21.64	27.73/138.66/277.32
2M19092321+4746226	Kepler-1049 b	611^{+132}_{-127}	1.163	29.17	0.52	0.275	0.033	720	63.63	2.95/14.77/29.53	37.84/189.21/378.41
2M19130013+4640465	Kepler-1350c	488^{+207}_{-183}	0.68	19.3	0.415	0.217	0.022	784	89.6	3.91/19.54/39.08	50.07/250.36/500.72
2M19130013+4640465	Kepler-1350 b	488^{+207}_{-183}	0.68	19.3	0.415	0.217	0.041	575	25.89	1.13/5.65/11.29	14.47/72.34/144.68
2M19213157+4317347	Kepler-138 e	444^{+114}_{-104}	0.698	18.86	0.465	0.245	0.18	293	1.73	0.06/0.3/0.61	0.78/3.9/7.8
2M19213157+4317347	Kepler-138 d	444^{+114}_{-104}	0.698	18.86	0.465	0.245	0.128	347	3.45	0.12/0.61/1.21	1.55/7.77/15.53
2M19213157+4317347	Kepler-138 c	444^{+114}_{-104}	0.698	18.86	0.465	0.245	0.091	413	6.87	0.24/1.21/2.41	3.09/15.46/30.92
2M19213157+4317347	Kepler-138 b	444^{+114}_{-104}	0.698	18.86	0.465	0.245	0.075	454	10.07	0.35/1.77/3.54	4.53/22.66/45.31
2M19301848+3907151	Kepler-1741 b	615^{+139}_{-135}	0.851	29.79	0.433	0.228	0.03	691	53.86	2.66/13.31/26.62	34.1/170.52/341.04
2M19312949+4103513	Kepler-45 b	580^{+154}_{-147}	1.209	15.8	0.535	0.281	0.03	775	85.29	3.93/19.64/39.27	50.32/251.61/503.22
2M19543665+4357180	Kepler-186 f	358^{+166}_{-141}	0.551	33.69	0.452	0.238	0.393	195	0.34	0.01/0.05/0.1	0.13/0.65/1.29
2M19543665+4357180	Kepler-186 e	358^{+166}_{-141}	0.551	33.69	0.452	0.238	0.122	350	3.57	0.11/0.53/1.05	1.35/6.74/13.47
2M19543665+4357180	Kepler-186 d	358^{+166}_{-141}	0.551	33.69	0.452	0.238	0.086	417	7.13	0.21/1.05/2.1	2.69/13.45/26.9
2M19543665+4357180	Kepler-186 c	358^{+166}_{-141}	0.551	33.69	0.452	0.238	0.058	510	16.02	0.47/2.36/4.72	6.05/30.23/60.46
2M19543665+4357180	Kepler-186 b	358^{+166}_{-141}	0.551	33.69	0.452	0.238	0.038	628	36.88	1.09/5.43/10.86	13.92/69.58/139.16
2M20004946+4501053	Kepler-560 b	708^{+419}_{-318}	0.576	50.47	0.291	0.151	0.092	321	2.52	0.19/0.97/1.94	2.49/12.46/24.92

Notes.

^a IHZ derived for planetary masses of $1 M_{\oplus}$.

^b For $r_M = 5R_p$, considering $f = 1\%$, 5% , and 10% .

^c For $r_M = 11.7R_p$, considering $f = 1\%$, 5% , and 10% .

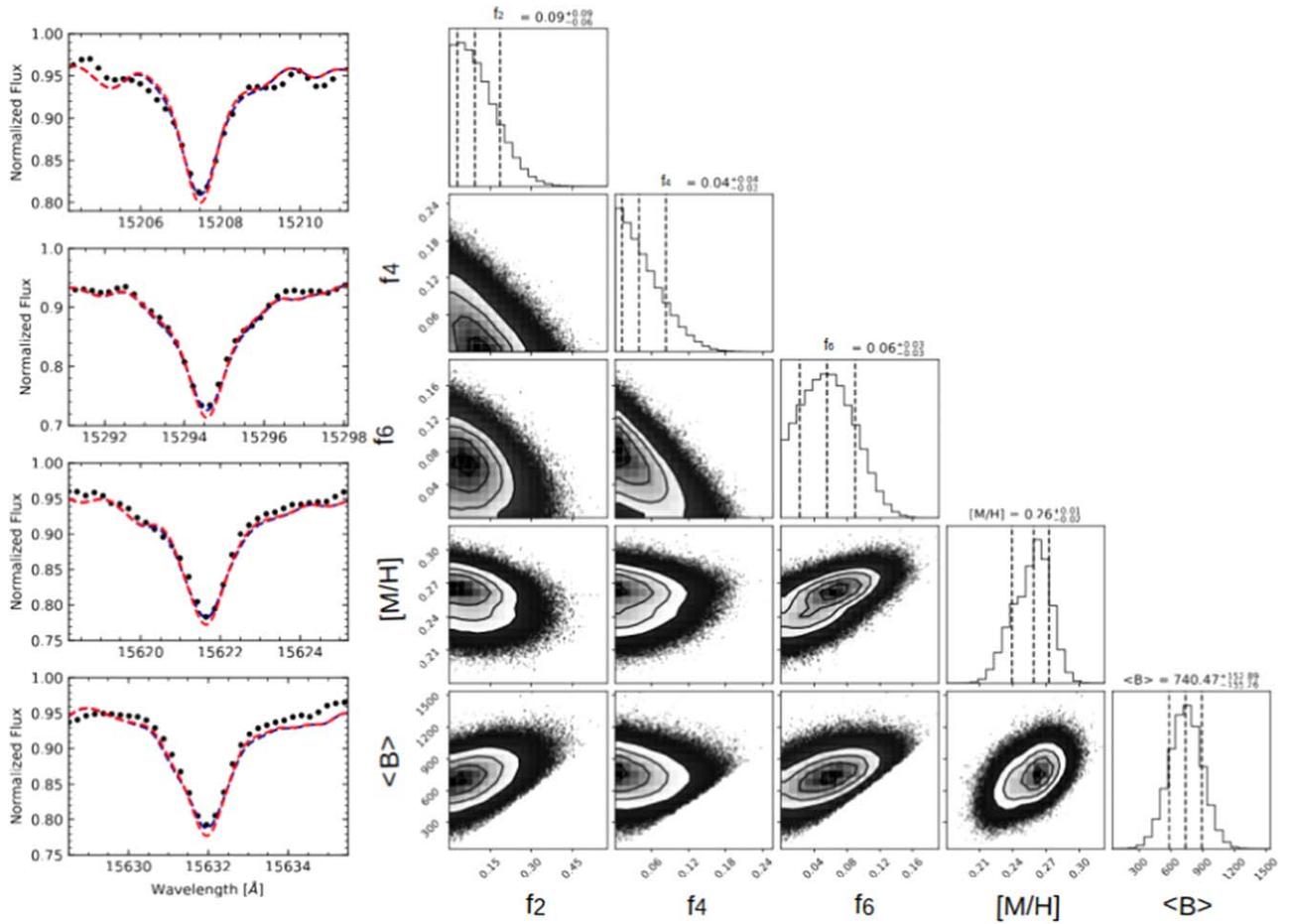


Figure 1. Magnetic field analysis for the star 2M07590587+1523294. The left panels show the four Fe I lines used in the modeling: black dots are the observed APOGEE spectrum, red dashed lines are synthetic profiles computed without a magnetic field, and dark blue lines are our best fits obtained from the Markov Chain Monte Carlo modeling. The right panel is a corner plot that presents the median and uncertainties (from 16th and 84th percentiles) of the derived parameters, which includes filling factors from magnetic fields between 2 and 6 kG in steps of 2 kG. We also show the final magnetic field result and its uncertainties.

lines are models computed with the exact same parameters as the blue lines, but without magnetic field. The right panel of Figure 1 shows the corresponding corner plot, with the posterior distribution for the filling factors and metallicity, as well as the posterior distribution for $\langle B \rangle$.

4. Discussion

4.1. Stellar Magnetic Fields and Stellar Rotation

The mean magnetic fields for the studied M dwarfs range between ~ 0.2 and ~ 1.5 kG. The distribution of the values for $\langle B \rangle$ from this study is presented as the blue histogram in Figure 2. For comparison, we also show in this figure a histogram (in orange) representing the distribution of the mean magnetic fields obtained for the sample of M-dwarf members of the young Pleiades open cluster studied by F. Wanderley et al. (2024), whose mean magnetic field results are on the same scale as those here. One can clearly see from the two distributions in Figure 2 that there is an evolution in the mean magnetic fields between the two samples. For the Pleiades, where $\text{age}_{\text{cluster}} \sim 10^8$ yr, the magnetic fields for the M dwarfs are characterized by a distribution having stronger mean B fields, with a peak at ~ 3 kG. For the M-dwarf sample of planet hosts in this study, on the other hand, the peak is at lower $\langle B \rangle$ values, roughly between 0.5 and 1 kG, with only two stars having $\langle B \rangle > 1$ kG. The differences between the mean

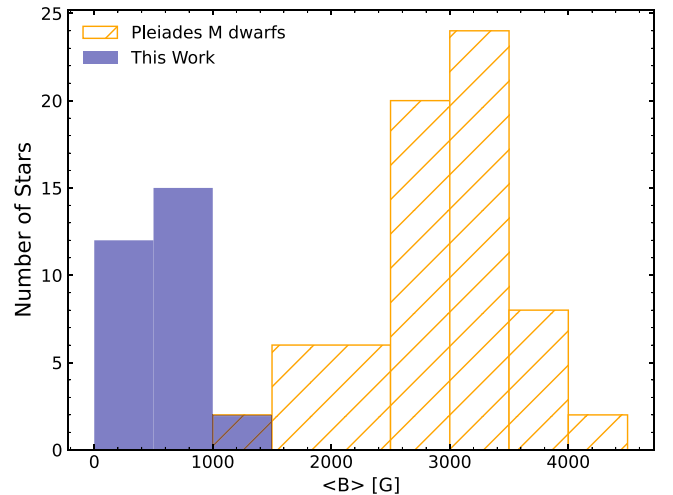


Figure 2. The distribution of the derived mean magnetic fields for the sample of M dwarfs studied here (blue histogram), and for a sample of M-dwarf stars belonging to the young Pleiades open cluster from F. Wanderley et al. (2024) (orange histogram).

magnetic field distributions of the two samples as a function of the stellar rotational periods will be further discussed below. But we note here, that the planet-hosting field M dwarfs in this study are likely much older than the Pleiades sample, based for

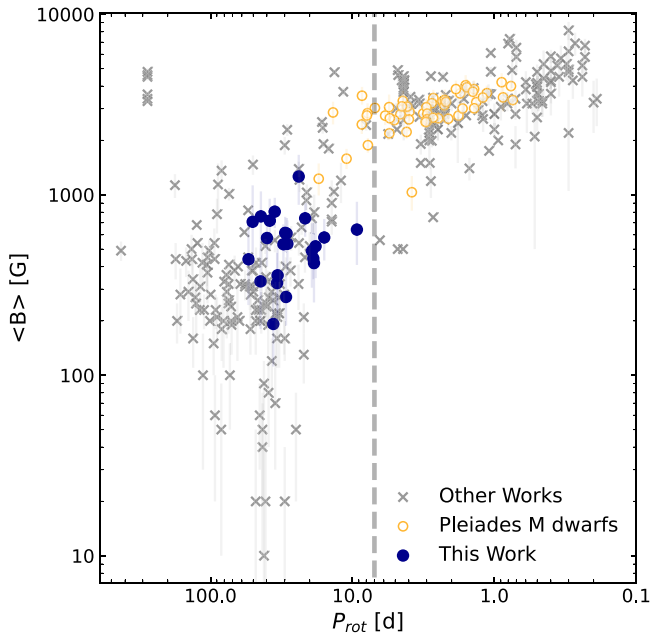


Figure 3. Derived mean magnetic fields for the sample of planet-hosting M dwarfs as a function of rotational periods (filled blue circles). Other results for M dwarfs from the literature are also shown (gray xs, S. H. Saar & J. L. Linsky 1985; S. H. Saar 1994, 1996; C. M. Johns-Krull & J. A. Valenti 1996, 2000; O. Kochukhov et al. 2001, 2009; N. Afram et al. 2009; N. Phan-Bao et al. 2009; D. Shulyak et al. 2011, 2014, 2017, 2019; O. Kochukhov & A. Lavail 2017; O. Kochukhov & D. Shulyak 2019; A. Reiners et al. 2022; P. I. Cristofari et al. 2023a, 2023b), along with results for a sample of Pleiades M-dwarf stars from F. Wanderley et al. (2024) (open orange circles). The gray dashed line at $P_{\text{rot}} = 7$ days represents the threshold that separates the saturated from the unsaturated regime. The mean magnetic fields for our sample fall in the unsaturated regime.

example, on the different distributions of their rotational periods (S. G. Engle & E. F. Guinan 2023).

The behavior of mean B fields as a function of stellar rotational periods (on a log–log scale) is shown in Figure 3. The literature magnetic field results exhibited in this figure (shown as gray xs) were all obtained from Zeeman split/intensified lines (S. H. Saar & J. L. Linsky 1985; S. H. Saar 1994, 1996; C. M. Johns-Krull & J. A. Valenti 1996, 2000; O. Kochukhov et al. 2001, 2009; N. Afram et al. 2009; N. Phan-Bao et al. 2009; D. Shulyak et al. 2011, 2014, 2017, 2019; O. Kochukhov & A. Lavail 2017; O. Kochukhov & D. Shulyak 2019; A. Reiners et al. 2022; P. I. Cristofari et al. 2023a, 2023b). The results from this study are shown as filled blue circles, with rotational periods taken from A. McQuillan et al. (2013a, 2013b), T. Mazeh et al. (2015), A. S. Bonomo et al. (2017), A. W. Mann et al. (2017), G. Torres et al. (2017), M. R. Kosiarek et al. (2019), E. A. Gilbert et al. (2020), T. Reinhold & S. Hekker (2020), P. Bluhm et al. (2021), and F. Murgas et al. (2023, 2024), and we also show, as open orange circles, mean magnetic field results for the Pleiades M dwarfs (F. Wanderley et al. 2024).

Figure 3 exhibits an inverse correlation between rotational periods and mean magnetic fields, which is steeper for stars with $P_{\text{rot}} > 7$ days and flatter for stars with shorter rotational periods. The steeper and flatter relations between $\langle B \rangle$ and P_{rot} define two regimes; younger stars that rotate faster are in the “saturated regime”, where $\langle B \rangle$ changes slowly as a function of P_{rot} , and where the stars approach a limit of kinetic to magnetic energy conversion (A. Reiners et al. 2022;

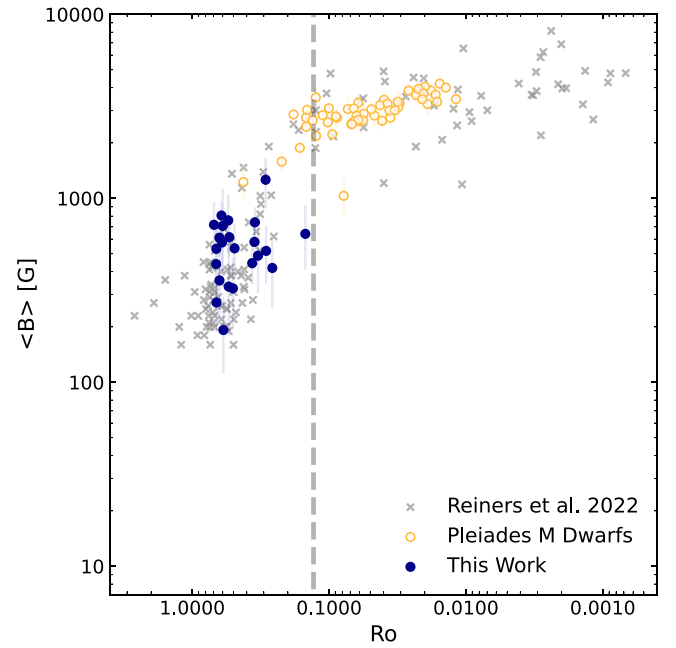


Figure 4. Derived mean magnetic fields for the sample of planet-hosting M dwarfs as a function of Rossby numbers (filled blue circles). Results for M dwarfs from A. Reiners et al. (2022) are shown (gray xs). The gray dashed line at $Ro = 0.13$ represents the threshold that separates the saturated from the unsaturated regime.

F. Wanderley et al. 2023), while older stars that rotate slower are in the “unsaturated regime”, where $\langle B \rangle$ decreases with the rotational period. Note that in the $\langle B \rangle$ – P_{rot} plane, the M-dwarf sample studied here falls in the unsaturated regime; these stars have effective temperatures in the range between ~ 3400 and ~ 4000 K and are partially convective. The gray dashed vertical line at $P_{\text{rot}} = 7$ days in Figure 3 represents the estimated threshold that separates the saturated and unsaturated regimes. We note again that, although we are using the same methodology to derive mean magnetic fields and analyzing M dwarfs within a similar effective temperature range as in the Pleiades study of F. Wanderley et al. (2024), the distribution of both results in the P_{rot} – $\langle B \rangle$ plane are quite different, with the field M dwarfs in this study being entirely in the unsaturated regime, while most Pleiades M-dwarf stars are in the saturated regime.

Figure 4 shows the relation between the derived mean magnetic fields as a function of Rossby numbers (filled blue circles). The Rossby number (Ro) is a dimensionless quantity that is given by the ratio between the stellar rotational period and convective turnover time (τ , measured in days) and is an important activity indicator. We derived Rossby numbers adopting the same methodology employed by F. Wanderley et al. (2024), using the relation $\tau = 12.3 \times (L/L_{\odot})^{-0.5}$ from A. Reiners et al. (2022). To derive luminosities we considered bolometric correction calibrations from A. W. Mann et al. (2015, 2016), and distances from C. A. L. Bailer-Jones et al. (2021). In Figure 4 we show the results for field M dwarfs from A. Reiners et al. (2022) (gray xs), with the gray dashed vertical line at $Ro = 0.13$ in the figure, representing the estimated threshold that separates the saturated and unsaturated regimes. We see a similar behavior in the observed relation between mean magnetic fields and rotational periods and mean magnetic fields and Rossby numbers, indicating that the studied sample

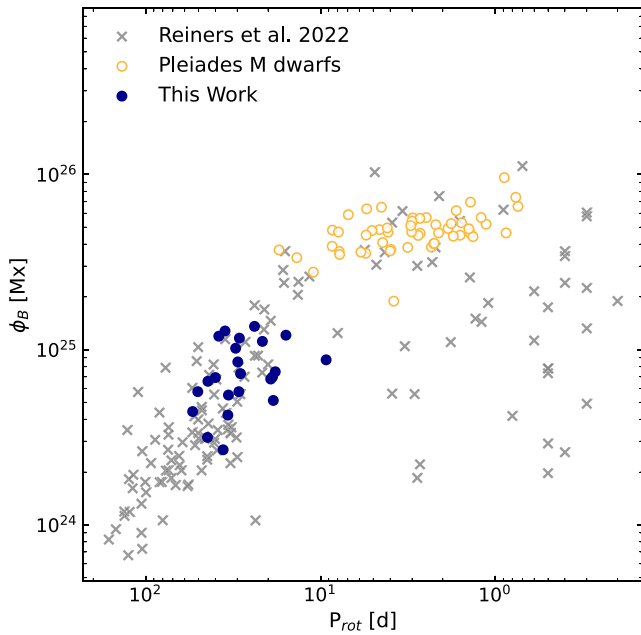


Figure 5. Derived magnetic fluxes for the studied M dwarfs as a function of their rotational periods (blue circles). The M-dwarf members of the young Pleiades open cluster (F. Wanderley et al. 2024; open orange circles) and for field M dwarfs (A. Reiners et al. 2022; gray xs) are also shown. The studied M dwarfs fall in the unsaturated regime and follow other results from the literature.

is composed of M-dwarf stars with nonsaturated magnetic fields, while the Pleiades M-dwarf stars are mostly saturated.

The segregation between the Pleiades M dwarfs and the planet-hosting field M dwarfs can be explained by the age difference between the two samples. The Pleiades stars have ages around 100 Myr (age = 112 ± 5 Myr; S. E. Dahm 2015), while the field star sample is likely much older and composed of stars that have dissipated much of their initial angular momentum, resulting in significantly smaller values of $\langle B \rangle$. S. G. Engle & E. F. Guinan (2023) quantified age–rotational period relations for M dwarfs and, according to that study, the values of $P_{\text{rot}} \sim 1$ –10 days that characterize the Pleiades sample span ages of one to a few hundred Myr, while the longer periods of $P_{\text{rot}} \sim 9$ –50 days that cover our planet-hosting field M-dwarf sample suggest ages of one to several Gyr.

We also derived magnetic fluxes in Mx units ($1 \text{ Mx} = 1 \text{ G} \times \text{cm}^2$) for our sample by multiplying mean magnetic fields and the stellar area, given by $4\pi R^2$. Figure 5 shows the magnetic fluxes for the sample stars as a function of their rotational periods as filled blue circles. We find an overall good agreement between the magnetic flux results in this study and those obtained for the field M dwarfs in A. Reiners et al. (2022) (gray xs), within the overlapping range in rotational periods, while the magnetic fluxes for the young M dwarfs from the Pleiades open cluster have lower rotational periods and much higher magnetic fluxes. We also note that, as pointed out in F. Wanderley et al. (2024), the magnetic fluxes for the young Pleiades M dwarfs show much less scatter than those for the field stars from the literature, which, again, may be explained by the age difference between both samples, as the field stars are not necessarily expected to have similar ages.

4.2. Planetary Habitability, Stellar and Planetary Magnetic Fields

As mentioned in the introduction, a star’s HZ is the region around it at which a planet would be able to maintain liquid water at its surface. Habitable zone calculations consider how planets process the thermal energy emitted by the host star. However, many other important features can drastically change habitability and ultimately significantly reduce the chances of finding life on a planet, in particular, for planets orbiting M dwarfs. Due to their lower thermal luminosity output, the habitable zones of exoplanets around M dwarfs are much closer to the star compared to those for hotter main-sequence stars. Therefore, there is a higher probability of tidal locking in such systems. Also, the typically high magnetic fields of M-dwarf stars, which for some cases in this study can be $\sim 1 \text{ kG}$, are responsible for both Extreme-UV (EUV) emission and X-ray nonthermal emission (N. Astudillo-Defru et al. 2017; E. R. Newton et al. 2017; N. J. Wright et al. 2018; O. Kochukhov 2021; A. Reiners et al. 2022; S. G. Engle 2024) as well as intense stellar winds that may erode or even evaporate planetary atmospheres. A planetary magnetic field would then be needed for planetary protection (J. Zendejas et al. 2010; A. A. Vidotto et al. 2013; V. See et al. 2014; J. D. J. do Nascimento et al. 2016; F. Gallet et al. 2017; J. M. Rodríguez-Mozos & A. Moya 2019; D. Veras & A. A. Vidotto 2021).

We start this discussion by investigating whether any of the exoplanets of the sample are inside the habitable zones of their stars. We used the 1D, radiative-convective, cloud-free climate model from R. K. Kopparapu et al. (2013). We adopted the “runaway greenhouse limit” and “maximum greenhouse limit” as, respectively, the inner (IHZ) and outer (OHZ) limits of the habitable zone. The model assumes H_2O - (IHZ) or CO_2 - (OHZ) dominated atmospheres with N_2 as a background gas. In the runaway greenhouse limit, water cannot condense into liquid droplets, and the stratosphere is dominated by water vapor, which suffers photolysis from stellar X-ray and EUV radiation, causing the loss of hydrogen, which results in an efficient mechanism for water loss (J. F. Kasting 1988). In the maximum greenhouse limit, the atmosphere is dominated by CO_2 , and the greenhouse effect is at its maximum, with each addition of CO_2 , only increasing the albedo, and cooling the planet. To derive the greenhouse limits, we used the equation below from R. K. Kopparapu et al. (2014):

$$d = \left(\frac{L/L_\odot}{S_{\text{eff}}} \right), \quad (2)$$

where d is the distance from the star given in astronomical units for either IHZ or OHZ. S_{eff} is the effective flux which is given by the equation:

$$S_{\text{eff}} = S_{\text{eff}\odot} + aT_* + bT_*^2 + cT_*^3 + dT_*^4, \quad (3)$$

where T_* is the stellar effective temperature minus the solar effective temperature of 5780 K. The coefficients used in Equation (3), as well as $S_{\text{eff}\odot}$, are given in Table 1 of R. K. Kopparapu et al. (2014), with the runaway greenhouse limits depending on the planetary mass, and coefficients given for three planetary masses of $0.1M_\oplus$, $1M_\oplus$, and $5M_\oplus$. (As discussed by R. K. Kopparapu et al. (2014), the habitable zone model depends on features such as planetary mass and the amount of background N_2 gas, and further work with 3D

climate models is needed to improve the calculation for habitable zones around different types of stars.)

We computed habitable zones for those exoplanets in our sample with available semimajor axis measurements (a) in the literature and found that only two of them lie inside their habitable zones. One of these exoplanets is the well-known planet Kepler-186f (E. V. Quintana et al. 2014), which is located at 0.386 au from its host star and sits comfortably inside its host star’s habitable zone, with OHZ = 0.452 au and IHZ = 0.229–0.252 au; we derived for this exoplanet a radius of $R_p = 1.18 R_\oplus$ (the same value from the DR25 KOI Table, S. E. Thompson et al. 2018), and depending on its planetary mass, Kepler-186f may be similar to the Earth. The other exoplanet from our sample that is in the habitable zone is TOI-700d (E. A. Gilbert et al. 2020). For this exoplanet, we derived a radius of $R_p = 1.16 R_\oplus$ (similar to the value of $R_p = 1.073 R_\oplus$ from E. A. Gilbert et al. 2023), and it has a distance from its host star of 0.163 au. If we consider that TOI-700d has a mass between 1 and 5 M_\oplus , it would be inside the habitable zone with IHZ = 0.153–0.158 au. If, on the other hand, this planet were much less massive, it would be out of the habitable zone, given that, for $M_p = 0.1 M_\oplus$, IHZ = 0.168 au.

We can also compute the insolation, S_p , i.e., the energy flux that a planet receives from its host star, using the equation

$$\frac{S_p}{S_\oplus} = \left(\frac{R_*}{R_\odot}\right)^2 \left(\frac{T_{\text{eff}*}}{T_{\text{eff}\odot}}\right)^4 \left(\frac{1 \text{ au}}{a}\right)^2, \quad (4)$$

where R_* is the stellar radius.

Another important exoplanet parameter is the equilibrium temperature T_{eq} , which is the temperature of the planet considering that all the absorbed energy is re-emitted as thermal radiation, i.e., the planet is neither cooling nor heating. The equilibrium temperature only considers heating by stellar radiation, and it does not account for other heating or cooling mechanisms such as, for example, the greenhouse effect. The planet’s equilibrium temperature is given by

$$T_{\text{eq}} = T_{\text{eff}}(1 - A)^{0.25} \sqrt{\frac{R_*}{2a}}, \quad (5)$$

where A is the planetary albedo, which we adopt here to be the Earth albedo of $A_\oplus = 0.3$ (P. R. Goode et al. 2001). The derived habitable zones, insolation levels, and equilibrium temperatures, along with the orbital semimajor axis of the studied exoplanets are presented in Table 1.

In Figure 6, we combine the quantities derived above for the studied exoplanets and show the insolation (top panel) and equilibrium temperatures (bottom panel) as a function of the semimajor axis of the orbit of the exoplanet. The exoplanets are color coded according to the mean magnetic field of the host stars in each case (see color bar). Most of the planets in our sample are closer to their host stars than the IHZ, which is probably related to detection biases since both the radial velocity and transit methods are much more sensitive to detecting planets that are closer to their host stars. The only two planets in our sample found to be in the habitable zone, Kepler-186f and TOI-700d (shown as filled symbols), are the ones suffering the lowest insolation and having the lowest equilibrium temperatures. In contrast, exoplanets in our sample that are closer to their stars receive higher insolation and have higher equilibrium temperatures, which contribute to them being out of the HZ.

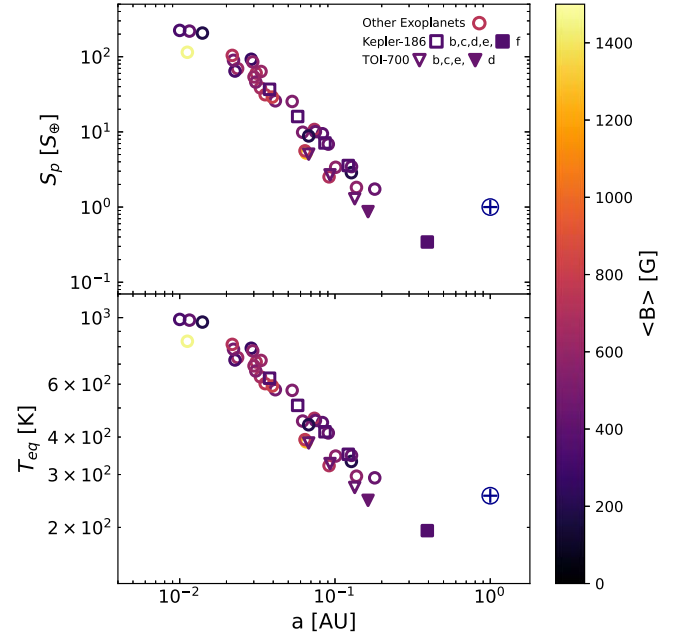


Figure 6. The top and bottom panels show, respectively, the insolation and equilibrium temperatures as a function of the orbit semimajor axis for the sample exoplanets. The exoplanets are color coded by the host star mean magnetic fields derived in this work; these are used to calculate the minimum planetary mass needed to protect the exoplanet from stellar winds. Most of the sample exoplanets are not in a habitable zone and these are shown as open symbols. The only exoplanets in the habitable zone of their stars are Kepler-186f (filled square) and TOI-700d (filled inverted triangle); the Earth is also shown for comparison.

Our measurements of the mean magnetic fields for the two stars in this sample that host planets in the HZ, Kepler-186 and TOI-700, can be used to estimate the impact of a magnetically driven wind on both Kepler-186f and TOI-700d. A. A. Vidotto et al. (2013) investigated the effect of magnetic fields from M-dwarf stars on the space environments around their planets and derived equations to estimate the minimum planetary magnetic fields required to deflect stellar wind pressure that is driven by stellar magnetic fields. We adopt the precepts of A. A. Vidotto et al. (2013) to estimate the minimum planetary B fields that would be needed to shield their surfaces, especially their atmospheres, from M-dwarf winds. We begin with the expression derived by A. A. Vidotto et al. (2013) for $P_{B*}(a)$, the magnetic pressure as a function of the orbital semimajor axis a (their Equation (6)):

$$P_{B*}(a) = \frac{B_{\text{SS}}^2}{8\pi} \left(\frac{R_{\text{SS}}}{a}\right)^4, \quad (6)$$

where B_{SS} is the stellar magnetic field evaluated at the source surface radius, R_{SS} . A. A. Vidotto et al. (2013) derived this expression using the potential field source surface (PFSS) method, which is valid for $a > R_{\text{SS}}$, and assumes that the stellar magnetic field decays with the square of the distance.

For a planetary surface or atmosphere to be shielded from a magnetized stellar wind, a sufficiently strong planetary magnetic field will be needed to balance the magnetic pressure from the stellar wind at some point away from the planet, which we call the magnetospheric radius, r_M . In the case of rocky terrestrial-type planets that orbit M dwarfs, it is expected that stellar magnetic pressure will dominate over stellar wind ram pressure, which will be ignored (e.g., A. A. Vidotto et al. 2011). The

equation below then describes the planetary magnetic pressure at a distance r_M from the planetary center (Equation (1) from A. A. Vidotto et al. 2013):

$$P_{Bp}(r_M) = \frac{[B_p(r_M)]^2}{8\pi}. \quad (7)$$

We assume a dipole field for a planetary magnetic field so that the field strength, B_p , at a distance r_M from the planetary center will have the form

$$B_p(r_M) = \frac{B_{p0}}{2} \left(\frac{R_p}{r_M} \right)^3, \quad (8)$$

where R_p is the planetary radius and B_{p0} is the planetary magnetic field strength at the pole. For the planetary magnetic field pressure to balance the stellar wind magnetic pressure at a distance, a , from the star and a distance, r_M , from the planet, then $P_{Bp}(r_M) = P_{B*}(a)$ and an expression for the requisite planetary magnetic field is:

$$B_{p,\min} = 2B_{SS} \left(\frac{R_{SS}}{a} \right)^2 \left(\frac{r_M}{R_p} \right)^3. \quad (9)$$

In Equation (9), R_{SS} , the launching radius for the stellar wind, is set to $2.5R_*$, as discussed in A. A. Vidotto et al. (2013), and the stellar magnetic field must be evaluated at R_{SS} . The mean stellar magnetic fields presented here are derived from Zeeman-broadened Fe I lines, which map small-scale fields integrated over the stellar surface, while the magnetic fields at $2.5R_*$ are expected to be dominated by the large-scale stellar magnetic field. As discussed by A. A. Vidotto et al. (2011) at the position of a planet, the large-scale component of the magnetic field (obtained from ZDI, for example) survives, while the small-scale magnetic fields (our determinations) do not. We estimated $\langle B_{ZDI} \rangle$ from our derived $\langle B \rangle$ for the star, considering the fraction $f = \langle B_{ZDI} \rangle / \langle B \rangle$ of these two stellar magnetic field characteristics derived in previous studies. O. Kochukhov (2021) provides a detailed review of magnetic fields in M-dwarf stars and compiles a list of stars with both small- and large-scale magnetic field measurements. As can be seen in Figure 15 in their work, for stars with $\langle B \rangle$ and mass values in the range of our sample ($\langle B \rangle \lesssim 1.5$ kG, and $M_* \gtrsim 0.4 M_\oplus$), the ratio between large- and small-scale magnetic fields never reaches $\sim 10\%$. Here, we examine a range of possibilities by determining $B_{p,\min}$ using $f = 1\%$, $f = 5\%$, and $f = 10\%$. We also assume a dipole-like behavior of the value of B_{SS} at $2.5R_*$, so that B measured at $R = 2.5R_*$ will be $0.051 \times \langle B \rangle$ at the stellar surface. Inserting these factors into Equation (9) results in the expression:

$$B_{p,\min} = 0.102f \times \langle B \rangle \left(\frac{2.5R_*}{a} \right)^2 \left(\frac{r_M}{R_p} \right)^3. \quad (10)$$

This expression can now be evaluated for the different values of f discussed above, as well as for different planetary magnetospheric radii, r_M/R_p . We considered magnetospheric radii based on the size of the Earth's magnetosphere today and 3.4 Gyr ago, which are respectively $r_M/R_p = 11.7$ and $r_M/R_p = 5$ (J. A. Tarduno et al. 2010). The derived $B_{p,\min}$ for all sample exoplanets are presented in Table 1.

Figure 7 shows the minimum magnetic planetary field, $B_{p,\min}$, as a function of the exoplanet semimajor axis, considering a present-day (top panel) and a young (bottom

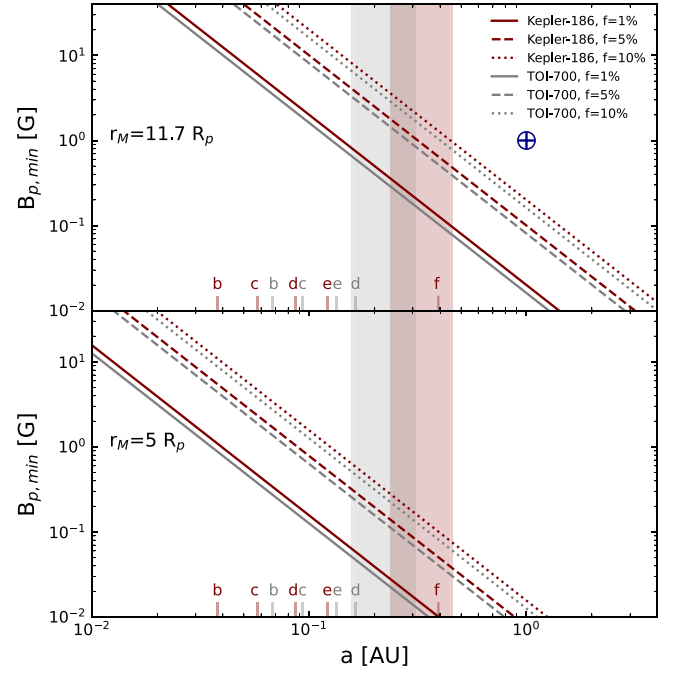


Figure 7. Minimum planetary magnetic fields for stellar winds deflection ($B_{p,\min}$) as a function of orbit semimajor axis (a). The top and bottom panels consider, respectively, magnetospheric sizes of $r_M = 11.7 R_p$ (Earth today) and $r_M = 5 R_p$ (Earth, 3.4 Gyr ago). The maroon and gray colors are associated with planetary systems of the stars Kepler-186 and TOI-700, respectively. The small vertical lines at the bottom of each panel show the semimajor axis of the exoplanets around these stars. The shaded regions represent the habitable zones for each star, with IHZ determinations based on a planetary mass of $1 M_\oplus$. Solid, dashed, and dotted lines are the $B_{p,\min}$ vs. a for each star, considering ratios between magnetic fields from circular polarimetry and intensity of respectively, 1%, 5%, and 10%. We also show the position of the Earth in the upper panel for comparison.

panel) Earth-size magnetosphere, for the two stars in our sample that host exoplanets inside habitable zones, Kepler-186 (represented in maroon) and TOI-700 (represented in gray). The small vertical lines and corresponding designating letters show the positions of the planetary systems in terms of the semimajor axis of their orbits. The maroon and gray shaded regions in the figure are the habitable zones of Kepler-186 and TOI-700, respectively, considering an IHZ for $1M_\oplus$ planetary mass. The inclined solid, dashed, and dotted lines are the $B_{p,\min}$ versus a relations computed using three different values for f (the ratio between magnetic fields obtained from ZDI to Zeeman enhanced spectral lines) of $f = 1\%$, $f = 5\%$, and $f = 10\%$. As previously concluded, we can see that only the exoplanets Kepler-186f and TOI-700d are inside the habitable zones of the stars, with the other exoplanets being too hot to sustain liquid water on the surface. For comparison, we show the position of the Earth in the upper diagram.

For a present-day Earth magnetosphere, assuming $r_M/R_p = 11.7$ (top panel of Figure 7), and taking the results for Kepler-186 of $\langle B \rangle = 358$ G, along with $R_* = 0.50 R_\odot$, and the distance for exoplanet Kepler-186f of $a = 0.386$ au, we find $B_{p,\min}$ values for $f = 1\%$, $f = 5\%$, and $f = 10\%$ of, respectively, 0.13 G, 0.65 G, and 1.29 G, indicating that for all cases, Kepler-186f would in principle be able to sustain an earth-sized magnetosphere if it had a magnetic field similar to the Earth. Doing the same estimate for the exoplanet TOI-700d, where $\langle B \rangle = 439$ G, $R_* = 0.41 R_\odot$, and $a = 0.163$ au, we obtain for $f = 1\%$, $f = 5\%$, and $f = 10\%$, $B_{p,\min}$ values of respectively

0.60 G, 3.02 G, and 6.04 G. TOI-700d would require larger minimum planetary magnetic fields than Kepler-186f and, in particular for the $f=5\%$ and $f=10\%$ cases, $B_{p,\min}$ is of a few times the magnetic field of the Earth.

If we now take the magnetosphere of the young Earth, around 3.4 Gyr ago, with a magnetospheric size of $r_M/R_p = 5$ (bottom panel of Figure 7), we obtain for Kepler-186, $B_{p,\min}$ values for $f=1\%$, $f=5\%$, and $f=10\%$, of respectively 0.01 G, 0.05 G, and 0.1 G. For these f ratios, it is not unreasonable to assume that the magnetic field of the exoplanet Kepler-186f is probably able to protect the planet and deflect coronal material from the host star. For TOI-700d we obtain a similar conclusion, with $B_{p,\min}$ values for $f=1\%$, $f=5\%$, and $f=10\%$, of respectively 0.05 G, 0.24 G, and 0.47 G.

As a final note, it is important to keep in mind that these estimations are based on a steady state, large-scale B field that drives stellar winds; stellar flares, large coronal mass ejections, and intense non-thermal radiation such as EUV and X-rays, which will impact habitability and planetary atmospheric and surface evolution, have not been considered.

5. Conclusions

As M-dwarf stars are the most abundant stellar type in our Galaxy and known to host more terrestrial-sized planets than their warmer main-sequence stellar siblings, they are interesting candidates in the search for planets having conditions that could possibly support life. Due to observations of strong magnetic fields around many M dwarfs, coupled with habitable zones (i.e., the region around a host star where liquid water can be sustained) that lie in close proximity to their host stars, stellar magnetic characterization of M dwarfs is a crucial step for understanding possible magnetic interactions between host stars and their planets. Magnetic fields are responsible for generating intense nonthermal EUV and X-ray radiation, as well as driving and controlling stellar winds, two processes that can impact the atmospheric evolution of orbiting planets (J. E. Owen & A. P. Jackson 2012; D. Modirrousta-Galian & J. Korenaga 2023).

In our previous study of M-dwarf members of the young Pleiades open cluster (F. Wanderley et al. 2024), we showed that the high-resolution ($R=22,500$), near-infrared (1.51–1.69 μm) SDSS APOGEE spectra could be used, in conjunction with the radiative transfer code Synmast (O. Kochukhov et al. 2010), to derive mean B -field strengths in these cool stars via Zeeman broadening of magnetically sensitive Fe I lines. Here, we extend this type of analysis to a sample of 29 planet-hosting M-dwarf field stars observed by the APOGEE survey, all of which have effective temperatures between ~ 3400 and ~ 4000 K. This particular M-dwarf sample hosts a total of 43 exoplanets, with 23 exoplanets detected by Kepler, nine exoplanets by K2, nine exoplanets by TESS, one exoplanet detected with the HARPS spectrograph, and another via TTV.

The results of our analysis of Zeeman-broadened lines found that our sample of M-dwarf planet hosts has measurable magnetic fields, with mean $\langle B \rangle$ fields ranging between $\langle B \rangle \sim 0.2$ and 1.5 kG. These mean magnetic fields for the sample stars are significantly weaker when compared to the ones obtained for the Pleiades M dwarfs in F. Wanderley et al. (2024). An investigation into the relation between mean magnetic fields, $\langle B \rangle$, as a function of stellar rotational periods (P_{rot}) found that all of the stars from the planet-hosting field

star sample with P_{rot} measurements lie in the nonsaturated regime. This is in contrast to the results for the Pleiades M dwarfs, where a large majority falls within the saturated area, and exhibits stronger mean B fields of $\langle B \rangle \sim 2\text{--}4$ kG, which can be explained by the young age of the cluster ($t_{\text{cluster}} \sim 10^8$ yr). The location of the Pleiades M dwarfs and the planet-hosting field M dwarfs studied here all fall within a locus in $\langle B \rangle$ versus P_{rot} defined by B -field measurements for other M dwarfs taken from the literature, suggesting that the planet-hosting M dwarfs do not have atypical mean magnetic fields. Similarly to mean magnetic fields, computed values for the mean magnetic fluxes, $\langle \phi_B \rangle$, for the studied M dwarfs also correlate with P_{rot} and also define both unsaturated and saturated regimes, in agreement with published values from the literature.

We also analyzed habitability for our sample of exoplanets by calculating the locations of their habitable zones (using prescriptions from R. K. Kopparapu et al. 2013), as well as equilibrium temperatures and insolation levels. We find that only two of the exoplanets in our sample are inside the habitable zones of their respective stars, Kepler-186f and TOI-700d. The remaining planets are outside, in regions with greater insolation levels and equilibrium temperatures that are too hot for water to condense into a liquid. However, although Kepler-186f and TOI-700d are inside their respective HZs, there are other effects aside from stellar thermal radiation that can compromise habitability in these systems, such as the effect of magnetic fields from the host M dwarfs.

Stellar magnetic fields provide important constraints on planet habitability. The mean stellar magnetic fields determined in this study were used to derive the minimum planetary magnetic field needed to protect the exoplanets from magnetically controlled stellar winds coming from the host M-dwarf star. We considered two scenarios based on A. A. Vidotto et al. (2013)’s framework, one that uses as a reference a present-day Earth magnetospheric size of $11.7 R_p$, and another that considers a magnetosphere of $5 R_p$, corresponding to a young Earth some ~ 3.4 Gyr ago.

In particular, we evaluated minimum planetary magnetic fields, $B_{p,\min}$, for those exoplanets in our sample that were inside their habitable zones, Kepler-186-f and KOI-700d. We investigated $B_{p,\min}$ assuming three different ratios ($f=1\%$, 5% , and 10%), between the large-scale magnetic field derived from circular polarimetry, $\langle B_{\text{ZDI}} \rangle$, which survives at the exoplanet’s position, and the small-scale magnetic field that we derive from Zeeman-broadened lines, $\langle B \rangle$, which does not survive at large distances from the stellar surface.

Assuming a magnetosphere corresponding to the present-day Earth, and a reasonable value for f of 5% (J. Morin et al. 2010; A. A. Vidotto et al. 2013; O. Kochukhov 2021), Kepler-186f would need a planetary magnetic field of 0.65 G to resist atmospheric stripping from stellar winds, which is smaller than the Earth’s present-day magnetic field of $0.25 \text{ G} \lesssim B \lesssim 0.65 \text{ G}$ (C. C. Finlay et al. 2010). The situation for the exoplanet TOI-700d, on the other hand, would be more difficult, as it would need a magnetic field of 3.02 G, which is around three times the Earth’s magnetic field, to protect the planet. If, however, we adopt the early Earth magnetosphere $r_M = 5 R_p$ as a reference, these values change for Kepler-186f and TOI-700d to, respectively, 0.05 G and 0.24 G, meaning that, in this scenario, both exoplanets would probably be able to shield their atmosphere from stellar winds. As a point of interest, 3.4 Gyr ago on the Earth there was an already established complex

biological carbon cycle in a marine ecosystem existing within this smaller magnetosphere (M. Reinhardt et al. 2024), which suggests that life might also develop in exoplanets in the habitable zone having such a magnetospheric size.

In conclusion, the results of this study suggest that the exoplanets Kepler-186f and TOI-700d possibly have the conditions necessary to maintain liquid water on their surfaces. In addition, given the measured mean magnetic fields of their host M dwarfs, the required planetary magnetic field needed to be able to shield these exoplanets from their host star winds due to intense magnetic fields is modest and not unreasonable for Earth-like planets, potentially making Kepler-186f and TOI-700d relevant for future exoplanetary habitability studies.












Acknowledgments

K.C. thanks Jeremy Drake for helpful discussions. F.W. acknowledges support from fellowship by Coordenação de Ensino Superior—CAPES. K.C. and V.S. acknowledge that their work here is supported, in part, by the National Science Foundation through NSF grant No. AST-2009507. O.K. acknowledges support by the Swedish Research Council (grant agreements No. 2019-03548 and 2023-03667), the Swedish National Space Agency, and the Royal Swedish Academy of Sciences. D.S. thanks the National Council for Scientific and Technological Development—CNPq. C.A.P. acknowledges financial support from the Spanish Ministry MICINN projects AYA2017-86389-P and PID2020-117493GB-I00. S.M. acknowledges funding from NASA XRP Grant 80NSSC24K0155. The Center for Exoplanets and Habitable Worlds is supported by the Pennsylvania State University and the Eberly College of Science. Funding for the Sloan Digital Sky Survey IV has been provided by the Alfred P. Sloan Foundation, the U.S. Department of Energy Office of Science, and the Participating Institutions. SDSS-IV acknowledges support and resources from the Center for High-Performance Computing at the University of Utah. The SDSS website is www.sdss.org. SDSS-IV is managed by the Astrophysical Research consortium for the Participating Institutions of the SDSS Collaboration including the Brazilian Participation Group, the Carnegie Institution for Science, Carnegie Mellon University, the Chilean Participation Group, the French Participation Group, Harvard-Smithsonian Center for Astrophysics, Instituto de Astrofísica de Canarias, The Johns Hopkins University, Kavli Institute for the Physics and Mathematics of the Universe (IPMU)/University of Tokyo, Lawrence Berkeley National Laboratory, Leibniz Institut für Astrophysik Potsdam (AIP), Max-Planck-Institut für Astronomie (MPIA Heidelberg), Max-Planck-Institut für Astrophysik (MPA Garching), Max-Planck-Institut für Extraterrestrische Physik (MPE), National Astronomical Observatory of China, New Mexico State University, New York University, University of Notre Dame, Observatório Nacional/MCTI, The Ohio State University, Pennsylvania State University, Shanghai Astronomical Observatory, United Kingdom Participation Group, Universidad Nacional Autónoma de México, University of Arizona, University of Colorado Boulder, University of Oxford, University of Portsmouth, University of Utah, University of Virginia, University of Washington, University of Wisconsin, Vanderbilt University, and Yale University.

Facility: Sloan.

Software: Matplotlib (J. D. Hunter 2007), Numpy (C. R. Harris et al. 2020), Synmast (O. Kochukhov et al. 2010), Turbospectrum (B. Plez 2012).

ORCID iDs

Fábio Wanderley  <https://orcid.org/0000-0003-0697-2209>
 Katia Cunha  <https://orcid.org/0000-0001-6476-0576>
 Verne V. Smith  <https://orcid.org/0000-0002-0134-2024>
 Oleg Kochukhov  <https://orcid.org/0000-0003-3061-4591>
 Diogo Souto  <https://orcid.org/0000-0002-7883-5425>
 C. Allende Prieto  <https://orcid.org/0000-0002-0084-572X>
 Suvrath Mahadevan  <https://orcid.org/0000-0001-9596-7983>
 Steven R. Majewski  <https://orcid.org/0000-0003-2025-3147>
 Philip S. Muirhead  <https://orcid.org/0000-0002-0638-8822>
 Marc Pinsonneault  <https://orcid.org/0000-0002-7549-7766>
 Ryan Terrien  <https://orcid.org/0000-0002-4788-8858>

References

- Abdurro'uf, Accetta, K., Aerts, C., et al. 2022, *ApJS*, **259**, 35
- Afram, N., Reiners, A., & Berdyugina, S. V. 2009, in ASP Conf. Ser. 405, Solar Polarization 5: In Honor of Jan Stenflo, ed. S. V. Berdyugina, K. N. Nagendra, & R. Ramelli (San Francisco, CA: ASP), 527
- Alvarado-Gómez, J. D., Drake, J. J., Garraffo, C., et al. 2020, *ApJL*, **902**, L9
- Alvarado-Gómez, J. D., Drake, J. J., Moschou, S. P., et al. 2019, *ApJL*, **884**, L13
- Astudillo-Defru, N., Delfosse, X., Bonfils, X., et al. 2017, *A&A*, **600**, A13
- Bailer-Jones, C. A. L., Rybizki, J., Fouesneau, M., Demleitner, M., & Andrae, R. 2021, *AJ*, **161**, 147
- Batalha, N. M., Rowe, J. F., Bryson, S. T., et al. 2013, *ApJS*, **204**, 24
- Belokurov, V., Penoyre, Z., Oh, S., et al. 2020, *MNRAS*, **496**, 1922
- Blanton, M. R., Bershad, M. A., Abolfathi, B., et al. 2017, *AJ*, **154**, 28
- Bluhm, P., Pallé, E., Molaverdikhani, K., et al. 2021, *A&A*, **650**, A78
- Bonomo, A. S., Desidera, S., Benatti, S., et al. 2017, *A&A*, **602**, A107
- Borucki, W. J., Koch, D., Basri, G., et al. 2010, *Sci*, **327**, 977
- Bowen, I. S., & Vaughan, A. H. J. 1973, *ApOpt*, **12**, 1430
- Cristofari, P. I., Donati, J. F., Folsom, C. P., et al. 2023a, *MNRAS*, **522**, 1342
- Cristofari, P. I., Donati, J. F., Moutou, C., et al. 2023b, *MNRAS*, **526**, 5648
- Dahm, S. E. 2015, *ApJ*, **813**, 108
- do Nascimento, J. D. J., Vidotto, A. A., Petit, P., et al. 2016, *ApJL*, **820**, L15
- Engle, S. G. 2024, *ApJ*, **960**, 62
- Engle, S. G., & Guinan, E. F. 2023, *ApJL*, **954**, L50
- Finlay, C. C., Maus, S., Beggan, C. D., et al. 2010, *GeoJI*, **183**, 1216
- Foreman-Mackey, D., Conley, A., Meierjürgen Farr, W., et al. 2013, emcee: The MCMC Hammer, Astrophysics Source Code Library, ascl:1303.002
- Gaia Collaboration, Prusti, T., de Bruijne, J. H. J., et al. 2016, *A&A*, **595**, A1
- Gaia Collaboration, Vallenari, A., Brown, A. G. A., et al. 2023, *A&A*, **674**, A1
- Gallet, F., Charbonnel, C., Amard, L., et al. 2017, *A&A*, **597**, A14
- Garraffo, C., Alvarado-Gómez, J. D., Cohen, O., & Drake, J. J. 2022, *ApJL*, **941**, L8
- Gilbert, E. A., Barclay, T., Schlieder, J. E., et al. 2020, *AJ*, **160**, 116
- Gilbert, E. A., Vanderburg, A., Rodriguez, J. E., et al. 2023, *ApJL*, **944**, L35
- Goode, P. R., Qiu, J., Yurchyshyn, V., et al. 2001, *GeoRL*, **28**, 1671
- Gunn, J. E., Siegmund, W. A., Mannery, E. J., et al. 2006, *AJ*, **131**, 2332
- Gupta, S., Basak, A., & Nandy, D. 2023, *ApJ*, **953**, 70
- Gustafsson, B., Edvardsson, B., Eriksson, K., et al. 2008, *A&A*, **486**, 951
- Harbach, L. M., Moschou, S. P., Garraffo, C., et al. 2021, *ApJ*, **913**, 130
- Harris, C. R., Millman, K. J., van der Walt, S. J., et al. 2020, *Natur*, **585**, 357
- Howard, A. W., Marcy, G. W., Bryson, S. T., et al. 2012, *ApJS*, **201**, 15
- Howell, S. B., Sobek, C., Haas, M., et al. 2014, *PASP*, **126**, 398
- Hunter, J. D. 2007, *CSE*, **9**, 90
- Johns-Krull, C. M., & Valenti, J. A. 1996, *ApJL*, **459**, L95
- Johns-Krull, C. M., & Valenti, J. A. 2000, in ASP Conf. Ser. 198, Stellar Clusters and Associations: Convection, Rotation, and Dynamos, ed. R. Pallavicini, G. Micela, & S. Sciortino (San Francisco, CA: ASP), 371
- Kasting, J. F. 1988, *Icar*, **74**, 472
- Klein, B., Donati, J.-F., Hébrard, É. M., et al. 2021, *MNRAS*, **500**, 1844
- Koch, D. G., Borucki, W. J., Basri, G., et al. 2010, *ApJL*, **713**, L79

- Kochukhov, O. 2021, [A&ARv](#), **29**, 1
- Kochukhov, O., Heiter, U., Piskunov, N., et al. 2009, in AIP Conf. Ser. 1094, 15th Cambridge Workshop on Cool Stars, Stellar Systems, and the Sun, ed. E. Stempels (Melville, NY: AIP), 124
- Kochukhov, O., & Lavail, A. 2017, [ApJL](#), **835**, L4
- Kochukhov, O., Makaganiuk, V., & Piskunov, N. 2010, [A&A](#), **524**, A5
- Kochukhov, O., Piskunov, N., Valenti, J., & Johns-Krull, C. 2001, in ASP Conf. Ser. 248, Magnetic Fields Across the Hertzsprung-Russell Diagram, ed. G. Mathys, S. K. Solanki, & D. T. Wickramasinghe (San Francisco, CA: ASP), 219
- Kochukhov, O., & Shulyak, D. 2019, [ApJ](#), **873**, 69
- Kopparapu, R. K., Ramirez, R., Kasting, J. F., et al. 2013, [ApJ](#), **765**, 131
- Kopparapu, R. K., Ramirez, R. M., SchottelKotte, J., et al. 2014, [ApJL](#), **787**, L29
- Kosiarek, M. R., Crossfield, I. J. M., Hardegree-Ullman, K. K., et al. 2019, [AJ](#), **157**, 97
- Kupka, F., Piskunov, N., Ryabchikova, T. A., Stempels, H. C., & Weiss, W. W. 1999, [A&AS](#), **138**, 119
- Majewski, S. R., Schiavon, R. P., Frinchaboy, P. M., et al. 2017, [AJ](#), **154**, 94
- Mann, A. W., Feiden, G. A., Gaidos, E., Boyajian, T., & von Braun, K. 2015, [ApJ](#), **804**, 64
- Mann, A. W., Feiden, G. A., Gaidos, E., Boyajian, T., & von Braun, K. 2016, [ApJ](#), **819**, 87
- Mann, A. W., Gaidos, E., Vanderburg, A., et al. 2017, [AJ](#), **153**, 64
- Mayor, M., Pepe, F., Queloz, D., et al. 2003, [Msngr](#), **114**, 20
- Mazeh, T., Perets, H. B., McQuillan, A., & Goldstein, E. S. 2015, [ApJ](#), **801**, 3
- McQuillan, A., Aigrain, S., & Mazeh, T. 2013a, [MNRAS](#), **432**, 1203
- McQuillan, A., Mazeh, T., & Aigrain, S. 2013b, [ApJL](#), **775**, L11
- Modirrousta-Galian, D., & Korenaga, J. 2023, [ApJ](#), **943**, 11
- Morin, J., Donati, J.-F., Petit, P., et al. 2010, [MNRAS](#), **407**, 2269
- Mulders, G. D., Pascucci, I., & Apai, D. 2015, [ApJ](#), **814**, 130
- Murgas, F., Castro-González, A., Pallé, E., et al. 2023, [A&A](#), **677**, A182
- Murgas, F., Pallé, E., Orell-Miquel, J., et al. 2024, [A&A](#), **684**, A83
- Newton, E. R., Irwin, J., Charbonneau, D., Berta-Thompson, Z. K., & Dittmann, J. A. 2016, [ApJL](#), **821**, L19
- Newton, E. R., Irwin, J., Charbonneau, D., et al. 2017, [ApJ](#), **834**, 85
- Nidever, D. L., Holtzman, J. A., Allende Prieto, C., et al. 2015, [AJ](#), **150**, 173
- Owen, J. E., & Jackson, A. P. 2012, [MNRAS](#), **425**, 2931
- Phan-Bao, N., Lim, J., Donati, J.-F., Johns-Krull, C. M., & Martín, E. L. 2009, [ApJ](#), **704**, 1721
- Piskunov, N. E., Kupka, F., Ryabchikova, T. A., Weiss, W. W., & Jeffery, C. S. 1995, [A&AS](#), **112**, 525
- Plez, B. 2012, Turbospectrum: Code for Spectral Synthesis, Astrophysics Source Code Library, ascl:1205.004
- Quintana, E. V., Barclay, T., Raymond, S. N., et al. 2014, [Sci](#), **344**, 277
- Reid, I. N., & Gizis, J. E. 1997, [AJ](#), **113**, 2246
- Reiners, A., Shulyak, D., Käpylä, P. J., et al. 2022, [A&A](#), **662**, A41
- Reinhardt, M., Thiel, V., Duda, J.-P., et al. 2024, [PreR](#), **402**, 107289
- Reinhold, T., & Hekker, S. 2020, [A&A](#), **635**, A43
- Ricker, G. R., Winn, J. N., Vanderspek, R., et al. 2015, [JATIS](#), **1**, 014003
- Rodríguez-Mozos, J. M., & Moya, A. 2019, [A&A](#), **630**, A52
- Saar, S. H. 1994, in Infrared Solar Physics, ed. D. M. Rabin, J. T. Jefferies, & C. Lindsey, Vol. 154 (Dordrecht: Kluwer), 493
- Saar, S. H. 1996, in Stellar Surface Structure, ed. K. G. Strassmeier & J. L. Linsky, Vol. 176 (Dordrecht: Kluwer), 237
- Saar, S. H., & Linsky, J. L. 1985, [ApJL](#), **299**, L47
- Salpeter, E. E. 1955, [ApJ](#), **121**, 161
- See, V., Jardine, M., Vidotto, A. A., et al. 2014, [A&A](#), **570**, A99
- Shields, A. L., Ballard, S., & Johnson, J. A. 2016, [PhR](#), **663**, 1
- Shulyak, D., Reiners, A., Engeln, A., et al. 2017, [NatAs](#), **1**, 0184
- Shkolnik, E. L., & Barman, T. S. 2014, [AJ](#), **148**, 64
- Shulyak, D., Reiners, A., Nagel, E., et al. 2019, [A&A](#), **626**, A86
- Shulyak, D., Reiners, A., Seemann, U., Kochukhov, O., & Piskunov, N. 2014, [A&A](#), **563**, A35
- Shulyak, D., Seifahrt, A., Reiners, A., Kochukhov, O., & Piskunov, N. 2011, [MNRAS](#), **418**, 2548
- Smith, V. V., Bizyaev, D., Cunha, K., et al. 2021, [AJ](#), **161**, 254
- Souto, D., Cunha, K., Smith, V. V., et al. 2020, [ApJ](#), **890**, 133
- Tarduno, J. A., Cottrell, R. D., Watkeys, M. K., et al. 2010, [Sci](#), **327**, 1238
- Thompson, S. E., Coughlin, J. L., Hoffman, K., et al. 2018, [ApJS](#), **235**, 38
- Torres, G., Kane, S. R., Rowe, J. F., et al. 2017, [AJ](#), **154**, 264
- Veras, D., & Vidotto, A. A. 2021, [MNRAS](#), **506**, 1697
- Vidotto, A. A., Jardine, M., Morin, J., et al. 2013, [A&A](#), **557**, A67
- Vidotto, A. A., Jardine, M., Morin, J., et al. 2014, [MNRAS](#), **438**, 1162
- Vidotto, A. A., Jardine, M., Opher, M., Donati, J. F., & Gombosi, T. I. 2011, [MNRAS](#), **412**, 351
- Wanderley, F., Cunha, K., Kochukhov, O., et al. 2024, [ApJ](#), **971**, 112
- Wanderley, F., Cunha, K., Souto, D., et al. 2023, [ApJ](#), **951**, 90
- Wilson, J. C., Hearty, F. R., Skrutskie, M. F., et al. 2019, [PASP](#), **131**, 055001
- Wright, N. J., Newton, E. R., Williams, P. K. G., Drake, J. J., & Yadav, R. K. 2018, [MNRAS](#), **479**, 2351
- Zendejas, J., Segura, A., & Raga, A. C. 2010, [Icar](#), **210**, 539